J Rubb Res, **2(3)**, 169–182

Molecular Conformation, Dynamics, and Chemical Shift Anisotropy of High Impact Polystyrene: Temperature Dependence and Stress Dependence Studies[†]

FAUZI MOHD SOM[*,**,#], JOHN A CHUDEK[*] AND GEOFFREY HUNTER[*]

Variable temperature and variable stress nuclear magnetic resonance spectroscopic and imaging studies are reported for a commercial sample of high impact polystyrene 'Liquid' nuclear magnetic resonance microscopy and 'solid' state stray field imaging studies indicated that imposed stress affects the molecular chain dynamics only of the polybutadiene region and not of the polystyrene (PS) matrix The molecular chain dynamics of the components of the composite were further studied by variable temperature relaxation time and chemical shift anisotropy (CSA) measurements The variable temperature (30°C – 210°C) ^1H spin-lattice relaxation time in the rotating frame ($T_{1\rho H}$) studies showed that up to 160°C the PS undergoes at least 2 different modes of motion, while at 95°C a change from asymmetric to axially symmetric in the CSA pattern of the aromatic ring ^{13}C-$\{^1H\}$ resonances revealed that the conformations of the phenyl rings are effectively locked below that temperature

High impact polystyrene (HIPS) is a composite material with a rubbery disperse phase In most of its industrial syntheses, bulk styrene monomer is polymerised in the presence of about 8% by weight of dissolved polybutadiene (PB), with or without the addition of small quantities of solvent and/or initiator[1] The process is homogeneous only up to about 6% of the monomer conversion, and thereafter heterogeneous From the beginning of the heterogeneous period until the point of phase inversion, the continuous phase is rich in the rubber, the disperse phase is practically pure polystyrene (PS) The phase inversion occurs at about 15% – 20% conversion and thereafter the matrix remains as the continuous phase The graft copolymer tends to accumulate at the interfaces, stabilising the heterogeneous mixture and favouring the phase inversion[2] The double bonds of PB do not participate directly in grafting or crosslinking in the thermal polymerisation of HIPS[2] As evidenced by electron microscopy, the elastomer phase of HIPS contains a large volume of PB droplets that consist of both grafted and ungrafted PS[3] A molecular interpretation of the domain has been reported[4]

PS alone is very brittle, but elastomer blending has been used with notable success in thermoplastics with the aim of obtaining tougher

---

[†] Paper presented at the International Rubber Conference 1997 Malaysia 6–9 October, Kuala Lumpur

[*] Rubber Research Institute of Malaysia, PO Box 10150, 50908 Kuala Lumpur Malaysia

[**] Department of Chemistry, University of Dundee, Dundee DD1 4HN, Scotland

[#] Corresponding author

polymers with greater impact resistance, albeit with some loss of rigidity and resistance to abrasion. Enhanced toughness resulting from increased grafting and reduced crosslinking has been reported[3].

A deformation can be induced by application of a stress or force on the sample. When such a deformation occurs in HIPS, crazing is the dominant energy absorbing mechanism[5], usually beginning at the crack tip. With the concentration of PB at around the commercial level of 8%, the craze bands in HIPS are, however, very diffused[5].

Nuclear magnetic resonance (NMR) has become a well established method to elucidate the structure and chain dynamics of polymers[6]. Applied to the study of polymers, NMR can be divided into four sections, namely: liquid state spectroscopy, solid state spectroscopy, 'liquid' imaging and solid imaging. In liquid state spectroscopy, only elastomer phases with significant chain mobility can be detected readily using high resolution methods. In solid state spectroscopy, the immobile components of polymers can also be detected with the aid of cross polarisation (CP), magic angle spinning (MAS), and high power proton decoupling.

Magnetic resonance imaging is achieved by applying a time-dependent linear magnetic field gradient to the sample[7]. The spatial resolution achievable is a function of both the magnitude of the magnetic field gradient and the inverse of the spin-spin relaxation time, T_2, which controls the line-width of the NMR signal. Sufficiently high gradients can usually be produced by conventionally switched coils to image satisfactorily the mobile components of an elastomer. Conventional 'liquid' magnetic resonance microscopy (NMRM) can therefore give spatial information of heterogeneities occurring in the sample, but only mobile components can be detected.

Immobile components give rise to signals with very short T_2's, requiring much higher field gradients for imaging. However, the emerging technique of stray field imaging (STRAFI), in which the large field gradient is provided by the fringe field of the superconducting coil of the spectrometer magnet can give spatial information about both immobile and marginally mobile components[8]. Therefore, in the context of the present study NMRM and STRAFI can be regarded as complementary techniques whereby both the polybutadiene and polystyrene phases can potentially be imaged.

In the study of polymer motions, various NMR relaxation parameters can be used[6], including the ^{13}C and ^{1}H spin-lattice relaxation times (T_{1C} and T_{1H})[9], the ^{1}H spin-spin relaxation time (T_{2H}), and the ^{1}H spin-lattice relaxation time in the rotating frame ($T_{1\rho H}$)[10,11]. Not all of these parameters provide direct information; nonetheless, the inferred information is important in characterising motional frequencies and amplitudes in solids.

The correlation time (τ_c) is a characteristic of the magnetisation decay attributed to a particular motion. For polymer chain motion, τ_c corresponds to the 'average' time for a bond rotation through one radian to occur.

An elastomer, at temperatures significantly above its glass transition temperature is very mobile and elastomer chain motions with frequency in the MHz region sensitively affect both T_1 and T_2. ^{1}H T_1 values for polymers are usually found to be single valued as the different T_1 values from different regions are averaged[12]. In contrast, ^{1}H T_2 values are usually multivalued, reflecting the number of

COPYRIGHT © MALAYSIAN RUBBER BOARD

phases occurring in the polymer[13] When motions are investigated by variable-temperature experiments, energies of activation, E_a, *(Equation 1)* can be obtained, each reflecting the different correlation times involved

$$\tau_c = \tau_0 e^{\left(\frac{E}{RT}\right)} \qquad 1$$

For rigid glassy polymers at temperatures well below their glass transition temperature (T_g), local motions with frequency in the kHz regime, involving side chain, terminal groups, or main-chain local fluctuations, dominate the relaxation behaviour[14 15] It has also been shown that when the polymer is under mechanical stress, the mechanism for avoiding local stress concentration is the dissipation of energy to the surroundings and it is therefore better detected by studying the low frequency motions[16] Such motions can be probed by variable-temperature $T_{1\rho}$ measurements

Relaxation in the rotating frame can be regarded as a competition between spin-spin relaxation (T_2) and spin-lattice relaxation (T_1) processes[17] If spin-lattice relaxation is the dominant process during cross polarisation, then $T_{1\rho}$ measurements will give a measure of molecular motion[18] The decay of ^{1}H magnetisation (M) as a function of contact time (τ) is given by *Equation 2* where T_{CH}, the cross relaxation time, is the time taken for the magnetisation to build up in the CP/MAS experiment

$$M_\tau = M_0\left(1-e^{\left(\frac{-\tau}{T_{CH}}\right)}\right)\left(e^{\left(\frac{-\tau}{T_{1\rho}}\right)}\right) \qquad 2$$

As shown in *Equation 3*, $T_{1\rho H}$ is related to the correlation time , the radio frequency of the spin lock field, ω_1, and the ^{13}C-^{1}H dipolar relaxation strength[19], B^2

$$\left(T_{1\rho}\right)^{-1} = \frac{B^2\tau_c}{1+\omega_1^2\tau_c^2} \qquad 3$$

A log plot of $T_{1\rho H}$ against the reciprocal of temperature (K^{-1}) reaches a minimum corresponding to *Equation 4*

$$\tau_c = \omega_1^{-1} \qquad 4$$

In the ^{13}C solid state spectrum, the sources of line broadening are largely dipolar interactions with nearby protons and chemical shift anisotropy, (CSA) High power ^{1}H decoupling eliminates the dipolar interactions, leaving CSA as the sole source of significant line broadening

The chemical shift is dependent on the orientation of the molecule in the spectrometer magnetic field and the complete three-dimensional shielding of the nucleus may be determined to give three principal shielding elements or shift tensors, σ_{11}, σ_{22}, and σ_{33} From these tensors the shielding anisotropy $\Delta\sigma$ *(Equation 5)* and the shielding asymmetry factor η (*Equation 6*) can be obtained

$$\Delta\sigma = \sigma_{33} - \frac{\sigma_{11}+\sigma_{12}}{2} \qquad 5$$

$$\eta = \frac{\sigma_{22}-\sigma_{11}}{\sigma_{33}-\sigma_{iso}} \qquad 6$$

Spinning the sample at the magic angle (MAS) of 54°44' to B_0 and at a rate greater than the CSA gives a single isotropic value for the chemical shift, σ_{iso} A manifold of spinning sidebands is observed at significantly lower spinning rates and their relative intensities can be used to extract the chemical shift tensors[20]

The signal to noise ratio can be substantially increased *via* cross polarisation (CP) which circumvents the long T_1's characteristic of solid materials The use of CP combined with slow MAS therefore allows the determination of the shift tensors of, e g carbon atoms of an organic molecule, particularly those of aromatic rings for whom large values of $\Delta\sigma$ and η might be anticipated[21 22]. As the motion increases, the CSA pattern evolves from asymmetric to axially symmetric, providing another means of detecting the onset of specific molecular motions in the polystyrene phase.

We now report variable temperature and variable stress NMR spectroscopic and imaging studies of the composite material, high impact polystyrene.

EXPERIMENTAL

Material

The sample of high impact polystyrene (produced by Athlone Extrusions Ltd., Republic of Ireland under the trade name of *Athpol 90*) was bought commercially as a sheet of dimension 2000×2000×3 mm.

Methods

Liquid state spectroscopy. Liquid state NMR spectroscopy was performed on a Bruker AM200 NMR spectrometer (^{1}H, 200.1; ^{13}C, 50.2 MHz) equipped with a variable temperature accessory. The HIPS was as a colloid in deuteriated chloroform ($CDCl_3$, $\delta(^1H)$, 7.24 p.p.m., $\delta(^{13}C)$, 77.0 p.p.m.; TMS, $\delta(^1H, {}^{13}C)$, 0.0 p.p.m.).

^{1}H spin-lattice relaxation times (T_{1H}) were measured by the inversion recovery method and ^{1}H spin-spin relaxation times (T_{2H}) by the use of Hahn spin echoes. The repetition delay used in both experiments was 10 secs.

Solid state spectroscopy. Solid state NMR spectroscopy was performed on a Chemagnetics CMX-300 Lite solids NMR spectrometer (^{1}H, 300.1; ^{13}C, 75.4 MHz) fitted with a Chemagnetics Pencil® MAS probe using 7 mm outside-diameter zirconia rotors. The spectrometer was equipped with a Chemagnetics variable temperature accessory. The sample was cut into small pieces and packed into the rotor. The experiment was performed by spinning at *ca.* 4500 Hz. The external reference used was adamantane (δ, 29.47 p.p.m. for the upfield peak[23]).

Both the $T_{1\rho H}$ and the CSA experiments used cross polarisation and magic angle spinning (CP/MAS) over temperatures ranging from 30°C–210°C. The experimental temperature was stabilised for 40 min before spectral accumulation.

In the determination of the shift tensors, lower spinning rates of *ca.* 500, 1000, 1500, 2000, 2500 and 3500 Hz were used. Although the contact time was initially set at 1.0 msec, at temperatures immediately below the observed $T_{1\rho H}$ minimum, more efficient cross polarisation was achieved with the contact time reduced to 0.5 msec; immediately above the minimum, the contact time was increased to 2.0 msec for greater CP efficiency. A pulse width of 3.8 μsec (90°) and a repetition delay of 10 sec were found to be adequate in the variable pulse delay experiment. The method described by Herzfeld and Berger[20] (HB) was used to calculate the shielding parameters from the relative intensities of the spinning sidebands.

Nuclear magnetic resonance microscopy. 'Liquid' nuclear magnetic resonance microscopy (NMRM) was performed using a Bruker AM300WB (89 mm bore magnet; ^{1}H, 300.1 MHz) NMR spectrometer fitted with a Bruker microimaging accessory. A 25 mm diameter cavity resonator RF coil was used. The sheet was cut into *ca.* 10 mm × 10 mm size pieces. They were individually compressed in a hydraulic press to 1, 2, 3, 4, 5, 6, 7, 8, 9 and 10 tons for one min and the compression then released A stack of one unstressed and ten stressed pieces was then assembled and bound together using cotton thread *(Figure 1)*

A standard Bruker three-dimensional spin-echo imaging sequence was used to accumulate the data which were subsequently processed using a Bruker Aspect X32 workstation The spin-echo image was accumulated with an echo time of 2 28 msec and a voxel size of 391 × 391 × 391 mm The field gradients used were G_x = 0 094 Tm ^{1}, G_y = 0 036 Tm ^{1}, G_z = 0 036 Tm ^{1}

Stray field imaging (STRAFI) The data were obtained using a Chemagnetics CMX-400 infinity console attached to a Magnex superconducting magnet of nominal field 9 4 T and a home built STRAFI probe-head located at the Department of Physics, University of Surrey In the fringe field accessed, B_0 was 5 57 T and the fringe field gradient was 58 Tm ^{1}

STRAFI images were obtained with a stack with unstressed HIPS at the top and HIPS compressed at 9 tons compression at the bottom A solid echo pulse sequence $\{(\pi/2)_x - \tau - [(\pi/2)_y - \tau -]_n$ Acquire$\}$ was used to accumulate the one dimensional image, where τ is the variable delay and n is the number of echoes The parameters used for that experiment were τ = 20 μsec, slice thickness = 250 μm, and 128 echo-trains for each slice The experiment was performed at ambient temperature (298 K) The data were processed by curve fitting each slice to *Equation 7*, where s and l refer to the short and long T_{2H} values, repsectively All curve fittings were performed with a commercial software package EasyPlot™[24]

$$M_\tau = M_{0\,s} e^{-\frac{\tau}{T_{2\,s}}} + M_{0\,l} e^{-\frac{\tau}{T}} \qquad 7$$

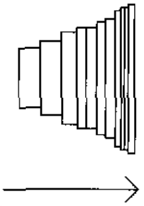

Figure 1 Drawing of a stack of compressed HIPS samples used for NMRM

RESULTS AND DISCUSSION

The T_2-weighted image of the stack clearly shows a decrease in image intensity *(Figure 2)* with increasing compression corroborating our initial findings[25]

A sharp decrease in image intensity was observed on moving from a compression of 1 ton to 2 tons The image intensity thereafter remained constant on greater compressions While there was no further reduction in image intensity the sample continued flowing upon further compression as showed by the continuing decrease in thickness *(Figures 1* and *3)*

Since NMRM is not capable of imaging the PS phase, the decrease in image intensity corresponds with a decrease in PB mobility which is consistent for an elastomer where the free volume is changed and segmental mobility reduced as it is stretched or stressed[26]

In the STRAFI imaging of a stack consisting only of an unstressed sample and one compressed at 9 tons *(Figure 4)*, T_{2H} values were extracted from the biexponentially decaying STRAFI echo trains and used to construct one-dimensional profiles The very short T_{2H} components (~ 50 μsec) was attributed to the PS region whereas the longer component (decreasing with increasing compression from ~ 16 msec to ~ 10 msec) was attributed to the soft domain which is the polybutadiene regime

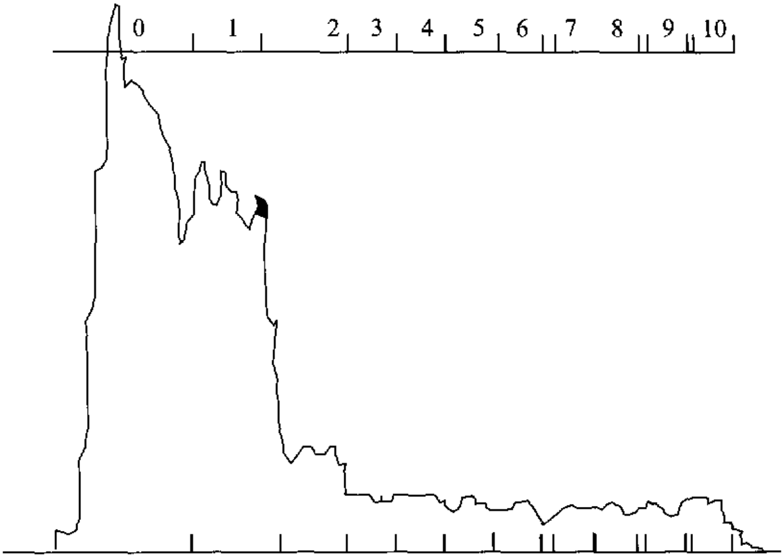

Figure 2 Image intensity profile of a T_2-weighted image of the stack The numbers represent the compression (tons) applied to individual sample of HIPS

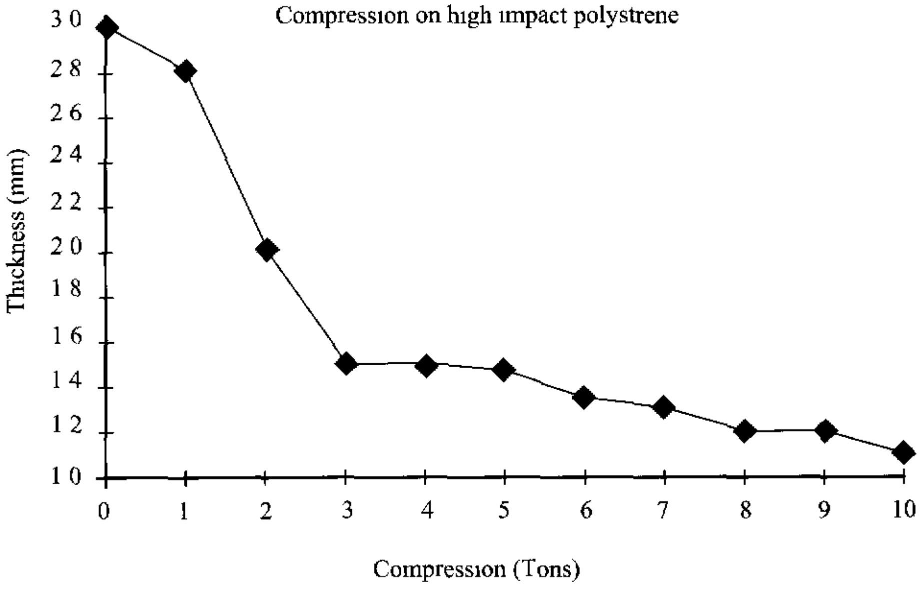

Figure 3 Plot of thickness of the samples against compression

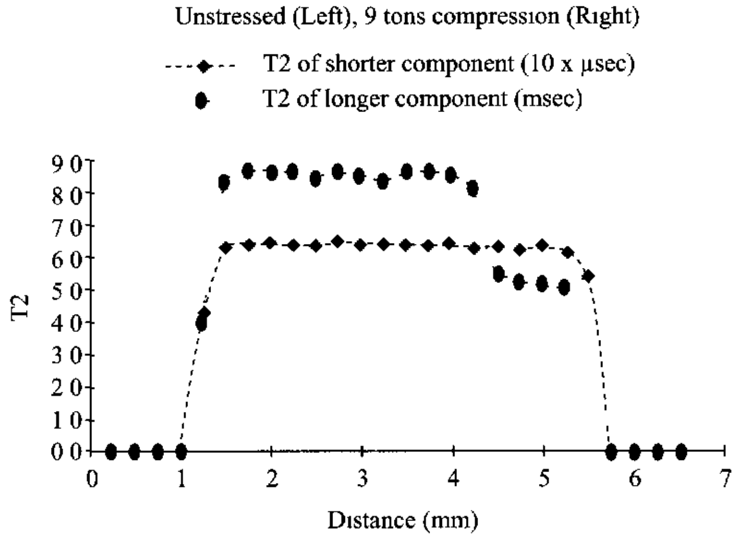

Figure 4 Plot of the T_{2H} *values from STRAFI experiments [♦ –* T_{2H} *of PS domain(s) (10 μ sec) and • –* T_{2H} *of PB domain(s) (m sec)]*

The boundary between the two samples is clearly delineated in the profile given by the longer T_{2H} component, but not in the profile given by the short T_{2H} component In addition to supporting the results found with NMRM, the STRAFI images showed clearly that PS mobility was not significantly affected by any compressive force imposed on the sample

It is clear that beyond a compression of 2 tons that either there is no remaining free volume in the PB domains, or that the physically entangled chains have been stretched to their maximum limits While the deformation with increasing compression is accommodated at the macroscopic level by flow of the HIPS, at the *microscopic* level the PS phase is not apparently affected at all It was therefore of interest to investigate in more detail the chain mobility behaviour of the PS phase, particularly as it is believed that for glassy polymers, deformation causes bond breaking, stretching or bending which further leads to cracking[27]

The ^{1}H and ^{13}C-{^{1}H} NMR spectra of HIPS are shown in *Figures 5* and *6*, respectively

Almost all of the anticipated peaks were observed Possible molecular structures for the PS matrix are shown in *Figure 7*

The PB content, as calculated from the ^{1}H NMR spectrum was 6 9% We found that the T_{1H} values for the HIPS colloid in $CDCl_3$ were consistent with those reported by others[28] The T_{2H} values are recorded in *Table 1* The spin-spin relaxation was biexponential, indicating that the different domains involved in the blend were retained in the colloid[28] The ^{1}H and ^{13}C-{^{1}H} NMR spectra of unsuspended HIPS obtained under 'liquid' spectroscopic conditions showed only signals arising from the PB microstructures.

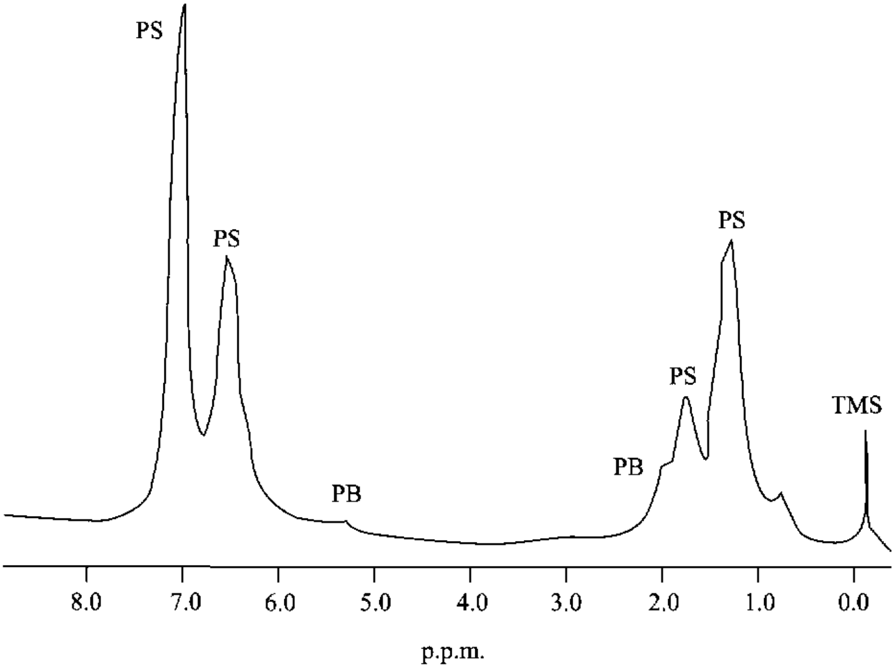

Figure 5. ^1H NMR spectrum of HIPS colloid in $CDCl_3$.

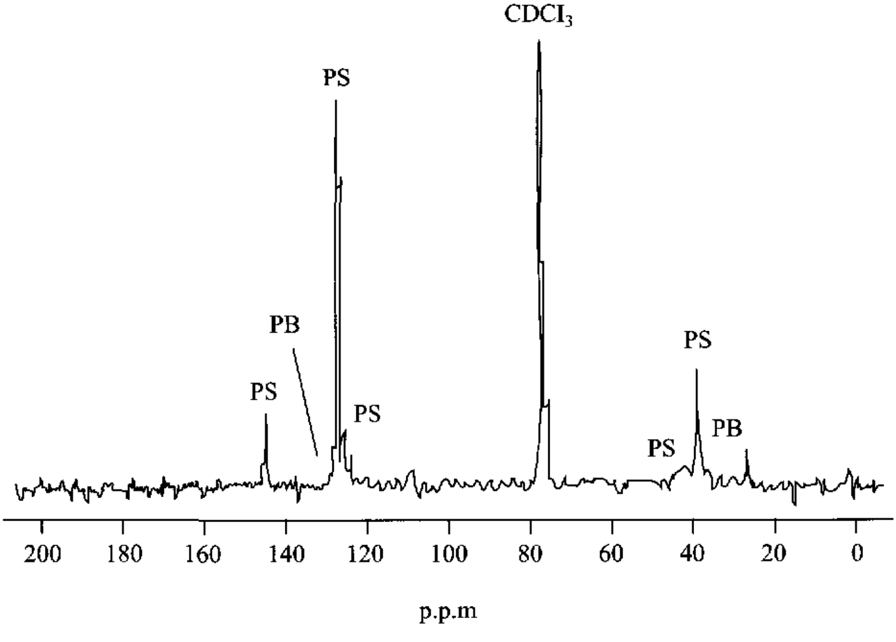

Figure 6. ^{13}C NMR spectrum of HIPS colloid in $CDCl_3$.

TABLE 1 T_{2H} VALUES FOR THE HIPS COLLOID

	T_{2H} (msec)	T_{2H} (msec)
PS(CH_2)	14	21
PS(CH)	11	25
PB(CH)	7	25
PS(o,o')	8	34
PS(m,m',p)	16	41

CP/MAS spectroscopy *(Figure 8)* was able to resolve the PS microstructure at the expense of the PB signals in two respects, firstly, the PB is very mobile rendering CP ineffective and secondly, the concentration of PB is low At long contact times the PB peaks, especially those from the carbons of the 1,4 double bonds became more apparent Even at a spinning rate of *ca* 4500 Hz *(Figure 8)*, the manifold of

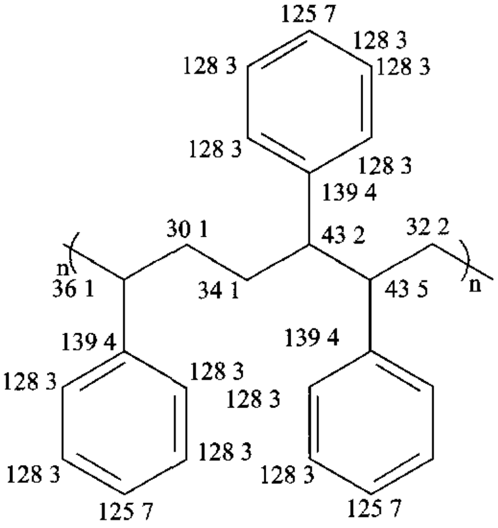

Figure 7 Possible structures of PS matrix with their assigned ^{13}C NMR chemical shifts

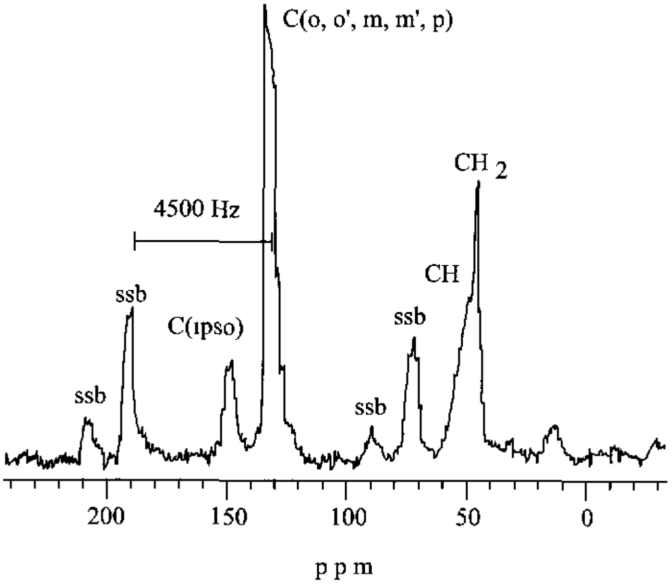

Figure 8 CP/MAS spectrum at v_r = 4500 Hz (ssb = spinning sidebands)

spinning sidebands showed the asymmetric condition of the aromatic ring carbons of the PS phase In the variable temperature CSA experiment, the spinning rate was reduced to increase the number of spinning sidebands as required for a more reliable analysis by the Herzfeld and Berger method *(Figure 9)*

We did not see any chemical shift anisotropic pattern for the carbon signals in the aliphatic region of the PS The CSA analysis of PS is therefore confined to the signals from the *ipso*, *ortho*, *meta*, and *para* carbons of the phenyl rings As shown in *Figure 10*, σ_{11} and σ_{22} converge towards each other with increasing temperature and a transition from an asymmetric to axially symmetric CSA pattern is ultimately observed The HB analysis was performed only up to 130°C as it became increasingly difficult to deconvolute the individual peaks at the higher temperatures At above glass transition temperature (190°C) the spectral dispersion of HIPS was improved by using very low spinning rates *(Figure 11)*

The plot of shielding anisotropy against inverse temperature is shown in *Figure 12* and reveals a sudden increase in motion at $T \geq 95$°C

In the $T_{1\rho H}$ experiment, the minima for all types of PS carbons (aromatic *and* aliphatic) occurred at the same temperature (*ca* 160°C), which is about 30°C lower than the glass transition temperature The τ_c found at the common minimum was 2 6 µsec Two apparent energies of activation (E_{a1}, and E_{a2}) for each type of carbon atom were extracted from the semilog plot of τ_c against the reciprocal of temperature *(Figure 13)* and are recorded in *Table 2* The clear implication is that all the carbon atoms are similarly affected by the molecular motions and that the backbone and pendant groups of the PS domain(s) move co-operatively as has been previously suggested by Paulaitis and Khare[29] The high values of E_{a1} indicate that there can be very little motion involving the complete polymer chain at the lower temperatures

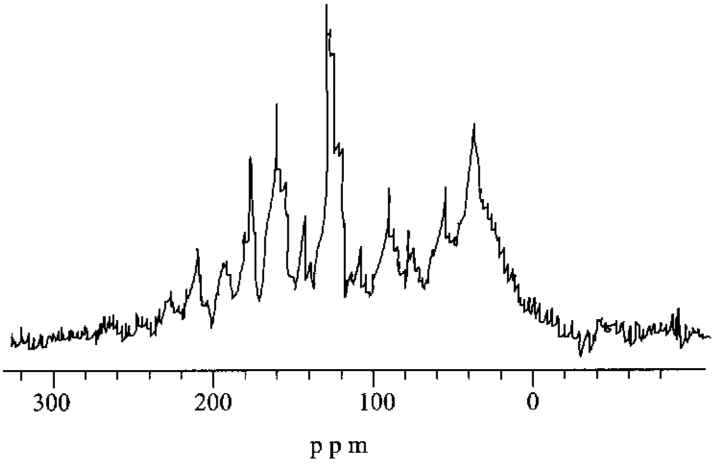

Figure 9 CPMAS spectrum (T = 35°C, ν_r = 2700 Hz)

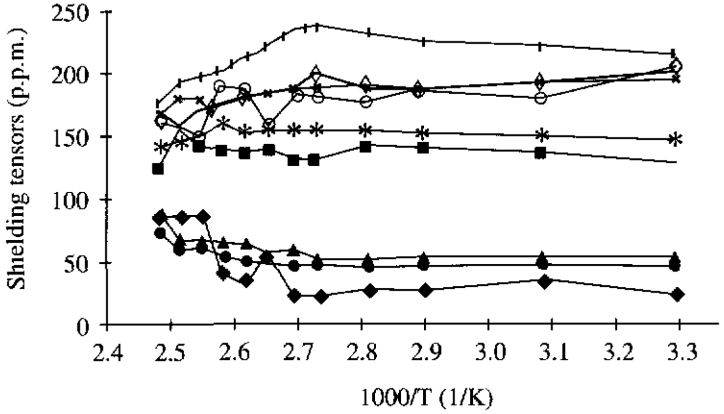

Figure 10 Shielding tensors (σ_{ii}) of the aromatic rings vs. *inverse of temperatures (Legends: σ_{11}, σ_{22}, σ_{33} of 146 p.p.m.: +, ○, ◇; 128 p.p.m.: x, *, ●; 126 p.p.m.: ◆, ■, ▲).*

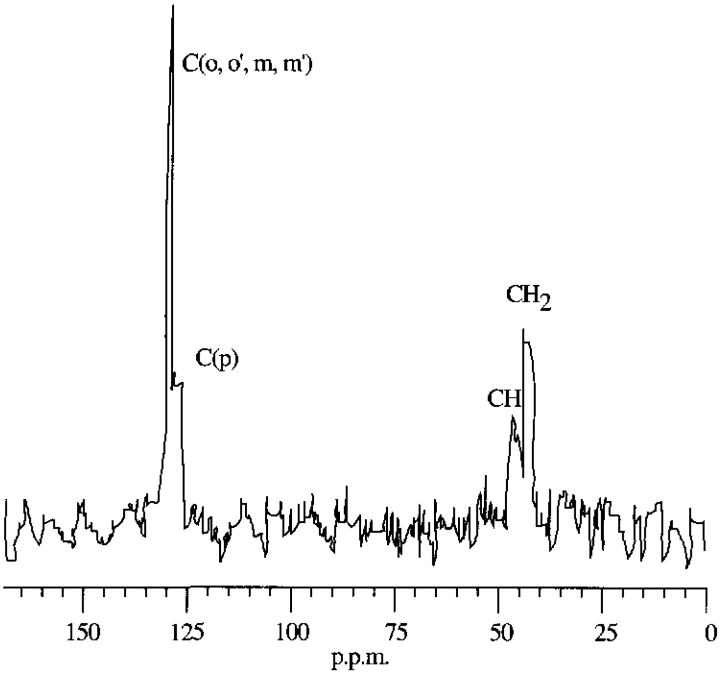

Figure 11. CPMAS spectrum ($T = 200°C$, $\nu_r = 247$ Hz).

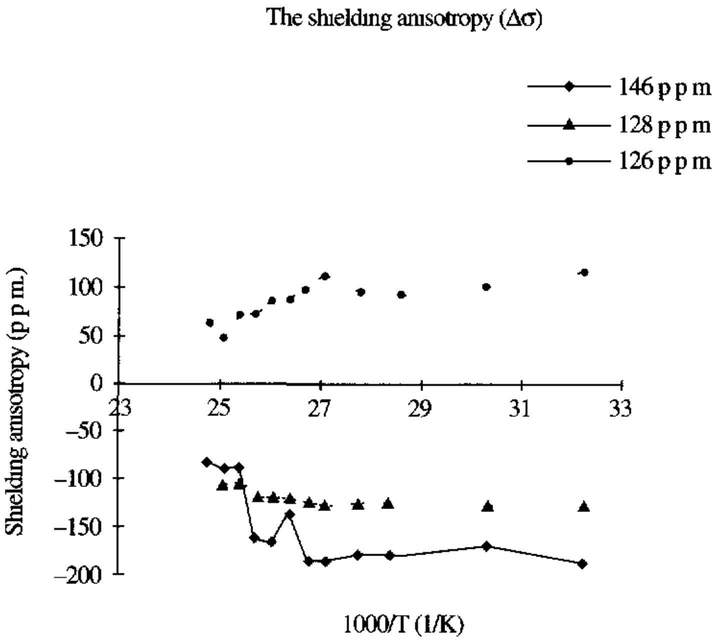

Figure 12 The shielding anisotropy (Δσ) of the aromatic rings at inverse of temperatures

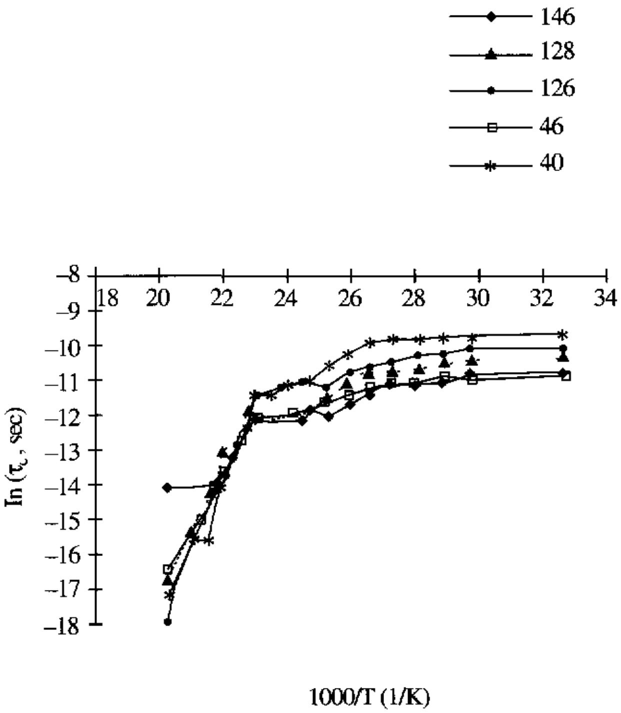

Figure 13 Natural log plot of the correlation times at inverse of temperatures

TABLE 2. E_a,S (kJmol^{-1}) FROM THE $T_{1\rho H}$ EXPERIMENTS

δ (p.p.m.)	$E_{a,1}$ (± 5%)	$E_{a,2}$ (± 10%)
41	99	17
46	146	33
126	116	22
128	117	25
146	81	17

CONCLUSION

Deformation of HIPS clearly affects the molecular motions of the PB domain(s). In contrast, the molecular mobility of the PS region is unaffected by such deformation and remains very restricted at ambient temperature. The restriction is probably imposed by the interlocking pendant groups and motion of these only becomes significant at temperatures above 95°C.

ACKNOWLEDGEMENTS

The Herzfeld Berger analysis program was obtained from Dalhousie University, Halifax, Nova Scotia, Canada. All STRAFI experiments were performed at the Department of Physics, University of Surrey, Guildford, England. We would like to thank Dr. Deirdre M. Lane, Dr. Benedict Newling and Dr. Peter J. McDonald for the STRAFI results. Financial support of the UK Engineering and Physical Sciences Research Council (EPSRC) (Grant No: GR/K12397) is gratefully acknowledged. The corresponding author would like to thank the Board of Rubber Research Institute of Malaysia (now known as the Malaysian Rubber Board) for the scholarship.

REFERENCES

1. AMOS, J.L. (1984) *Polym. Eng. Sci.*, **14**, 1.
2. PENG, F.M. (1990) *J. App. Polym. Sci.* **40**, 1289.
3. BUCKNALL, C.B. (1977) *Toughened Plastics.* London: Applied Science.
4. FISCHER, M., AND HELLMANN, G.P. (1996) *Macromolecules*, **29**, 2948.
5. MILES, I.S., AND ROSTAMI, S. (1992) *Multi-component Polymer Systems*, Polymer Science and Technology Series. London: Longman scientific and Technical, Chp 5.
6. McBRIERTY, V.J., AND DOUGLASS, D.C. (1980) *Physics Report* **63(2)**, 61.
7. CALLAGHAN, P.T. (1991) *Principles of Nuclear Magnetic Resonance Microscopy.* Oxford: Clarendon Press.
8. McDONALD, P.J. (1997) *Prog. NMR Spect.*, **30**, 69.
9. FENG, H., FENG, Z., RUAN, H. AND SHEN, L. (1992) *Macromolecules* **25**, 5981.
10. SCHAEFER, J., STEJSKAL, E.O. AND BUCHDAHL, R. (1977) *Macromolecules* **10**, 384.
11. VANDERHART, D.L., AND GARROWAY, A.N. (1979) *J. Chem. Phys.*, **71**, 2773.
12. PACKER, K.J., AND POPE, J.M. (1984) *J. of Poly. Sci.: Poly. Phys. Ed.*, **22**, 589.
13. CHARLESBY, A. (1976) *Rad. Phys. Chem.*, **8**, 557.
14. SCHAEFER, J., STEJSKAL, E.O., STEGER, T.R., SEFCIK, M.D. AND MCKAY, R.A. (1980) *Macromolecules*, **13**, 1121
15. BAYER, E., ALBERT, K. WILLISCH, H. RAPP, W., AND HEMMASI, B. (1990) *Macromolecules*, **23**, 1937.

16 TONELLI, A (1972) *Macromolecules,* **5**, 558

17 YANNONI, C S (1982) *Acc Chem Res* , **15**, 201

18 BOVEY, F A AND JELINSKI, W (1985) *J Phys Chem* , **89(4)**, 578

19 RIDDELL, F G , ARUMUGAM, S , HARRIS, K D M , ROGERSON, M AND STRANGE, J H *(1993) J Am Chem Soc* , **115**, 1881

20 HERZFELD, J AND BERGER, A E (1980) *J Chem Phys* , **73**, 6021

21 PAUSAK, S , TEGENFELDT, J AND WAUGH, J S (1974) *J Chem Phys* , **61**, 1338

22 VAN DONGEN TORMAN,J AND VEEMAN, W S (1978) *J Chem Phys* , **68**, 3233

23 HAYASHI, S AND HAYAMIZU, K (1991) *Bull Chem Soc Jpn* , **64**, 685

24 EasyPlot™, Spıral Software, USA

25 HUNTER, G AND CHUDEK, J A (1992) *J Mat Scı Lett* , **11**, 222

26 BLUMLER, P AND BLUMICH, B (1993) Acta *Polymer*, **44**, 125

27 SEYMOUR, R B AND CARRAHER, C E (1987) *Polymer Chemıstry* Marcell Dekker Inc

28 SEGRE, A L , CAPITANI, D , *et al* (1992) *Eur Polym J* , **28(10)**, 1165

29 KHARE, R AND PAULAITIS, M E (1995) *Macro-molecules*, **28**, 4495